Electronic properties of the tight-binding Fibonacci Hamiltonian

1989 J. Phys. A: Math. Gen. 22 951

(http://iopscience.iop.org/0305-4470/22/8/012)

J. Phys. A: Math. Gen. 22 (1989) 951-970. Printed in the UK

Electronic properties of the tight-binding Fibonacci Hamiltonian

Godfrey Gumbs and M K Ali

Department of Physics, University of Lethbridge, Lethbridge, Alberta, T1K 3M4 Canada

Received 5 May 1988

Abstract. The analysis of the electronic properties of the tight-binding Fibonacci Hamiltonian is carried out here using dynamical systems techniques. Two classes of Fibonacci sequences are considered, corresponding to the cases when there are two types of building blocks and also when there are three types of building blocks. The recursion relations for the traces of the transfer matrices are determined and studied for various extensions of the Fibonacci case with the golden mean. Some differences are obtained between the various types of second-order Fibonacci sequences and are most likely due to long-range order. Applications of this work to the transmission of light through a multilayered medium and the electrical resistance of a one-dimensional quasicrystal, as determined by the Landauer formula, are presented.

1. Introduction

The dynamical map for the trace of the transfer matrices has been rigorously explored in a number of papers. The interest in this problem has so far been mainly concerned with the tight-binding Schrödinger equation for which either the potential energy or kinetic energy terms take on two values arranged in a Fibonacci sequence with the golden mean [1-19]. The Fibonacci series with the golden mean is one example of a generalisation of sequences recently introduced by the authors [20-22]. In this paper, we explore these maps and discuss some examples which might be verified experimentally.

In this investigation, we consider two cases where the building blocks of the Fibonacci sequence take on (*a*) one of *two* values A and B, and (*b*) one of *three* values A, B and C. For the binary sequence, the sequence of As and Bs is the Fibonacci sequence S_∞, which is constructed recursively as

$$S_{l+1} = [S_{l-1}^m S_l^n] \tag{1}$$

for $l \geqslant 2$ and m and n are positive integers. For the ternary sequence, the recursion relation for the sequence of As, Bs and Cs is

$$S_{l+1} = [S_{l-2}^m S_{l-1}^n S_l^p] \tag{2}$$

where m, n and p are also positive integers. The initial conditions will be presented in the text. The tight-binding non-diagonal Schrödinger equation is

$$t_{l+1}\psi_{l+1} + t_l\psi_{l-1} = E\psi_l \tag{3}$$

0305-4470/89/080951+20$02.50

where ψ_l denotes the wavefunction at the lth site and $\{t_l\}$ are the hopping matrix elements. The diagonal version of this equation is

$$\psi_{l+1}+\psi_{l-1}+V_l\psi_l = E\psi_l \tag{4}$$

where $\{V_l\}$ are the values which the potential energy can have. Various studies have been made of the electronic spectra of a quasiperiodic model. It has been shown that the spectra are singular continuous for a class of Fibonacci lattices. In this case, the wavefunctions are *critical* and are in a sense intermediate between localised and extended states. Other cases of a singular continuous spectrum have been demonstrated by Hofstadter [23] and Avron and Simon [24].

We investigate (3) and (4) using dynamical systems techniques first introduced by Kohmoto *et al* [1] and adopted by many others. Scaling properties of the electronic states and the energy spectrum are discussed. Several new dynamical maps are introduced and analysed. The eigenvalues of the Jacobian matrices of transformation for these maps reveal some effects related to the quasiperiodicity of the sequences.

In § 2 the method of Kohmoto *et al* is applied to some examples of second-order Fibonacci series to obtain the dynamical maps and Cantor set spectra. The critical wavefunctions are also discussed in this section and we also examine the varying degrees of disorder by calculating the eigenvalues of the linearised dynamical mappings. In § 3, the quasiperiodic dynamics of a third-order Fibonacci lattice is examined. Section 4 contains a calculation of the transmission coefficient for light through various types of Fibonacci lattices. Section 5 deals with a calculation of the resistance of a quasicrystal given by the Landauer formula. A summary of our results is given in § 6.

2. Dynamical maps, energy spectra and invariants for second-order Fibonacci series

In this section, we derive the dynamical system described by a map for various types of Fibonacci series which are constructed according to (1). Both the off-diagonal model of (3) and the diagonal model of (4) are considered in our calculations. The quasiperiodic Schrödinger equation (4) can be written as

$$\begin{pmatrix}\psi_{l+1}\\ \psi_l\end{pmatrix} = \boldsymbol{M}(l)\begin{pmatrix}\psi_l\\ \psi_{l-1}\end{pmatrix} \tag{5a}$$

where the transfer matrix is given by

$$\boldsymbol{M}(l) = \begin{pmatrix}E-V_l & -1\\ 1 & 0\end{pmatrix}. \tag{5b}$$

The values of the wavefunctions at arbitrary lattice sites are obtained by repeatedly applying (5a) which gives

$$\begin{pmatrix}\psi_{N+1}\\ \psi_N\end{pmatrix} = \boldsymbol{M}(N)\boldsymbol{M}(N-1)\ldots\boldsymbol{M}(2)\boldsymbol{M}(1)\begin{pmatrix}\psi_1\\ \psi_0\end{pmatrix}. \tag{6}$$

We have thus reduced the problem to calculating products of unimodular (determinant equal to unity) 2×2 matrices. For the second-order Fibonacci lattices, the potential V_l has values V_A and V_B. If N is a Fibonacci number given by the recursion relation $F_{l+1} = mF_{l-1}+nF_l$ where m and n are positive integers, $\boldsymbol{M}_l$ is defined by

$$\boldsymbol{M}_l = \boldsymbol{M}(F_l)\boldsymbol{M}(F_l-1)\ldots\boldsymbol{M}(2)\boldsymbol{M}(1). \tag{7}$$

Since a Fibonacci sequence is constructed by (1), the matrix $\boldsymbol{M}_l$ on the Fibonacci sublattice, i.e. the Fibonacci number sites, is given by the recursion formula

$$\boldsymbol{M}_{l+1} = \boldsymbol{M}_{l-1}^m \boldsymbol{M}_l^n \tag{8}$$

for $l \geqslant 1$ with $\boldsymbol{M}_0 = \boldsymbol{M}_B$ and $\boldsymbol{M}_1 = \boldsymbol{M}_A$. The matrix recursion relation given by (8) can be interpreted as a kind of renormalisation group equation. As a matter of fact, Niu and Nori [25] have presented a renormalisation group approach based on novel decimation techniques which could be used as an alternative to study such systems. The Fibonacci sequence in (8) could be constructed by the inflation transformation $B \to A'$, $A \to B'^m A'^n$ where A^n is a string of n A. Subsequently, the transfer matrix is transformed according to $\boldsymbol{M}_l(A, B) \to \boldsymbol{M}_{l+1}(A', B')$ where $\boldsymbol{M}_l(A, B)$ is a product of F_l matrices arranged in a Fibonacci sequence as in (7) and $\boldsymbol{M}_{l+1}(A', B')$ is given in a similar way.

We now obtain the energy spectrum for an infinite lattice made up of a block of A and B arranged in a Fibonacci sequence, with periodic boundary conditions. The energy spectrum is defined by those values of the energy for which the corresponding wavefunctions are bounded. This is satisfied when the eigenvalues of $\boldsymbol{M}_l$ are complex with a magnitude of unity as $l \to \infty$. Since the matrix $\boldsymbol{M}_l$ is unimodular, this condition could be transferred to the trace which must satisfy $|\mathrm{Tr}\, \boldsymbol{M}_l| < 2$, as $l \to \infty$. Delyon and Petritis [15] proved that this model cannot have localised states. We now obtain a reduced dynamical system for the spectrum of several second-order Fibonacci sequences. Since the lattice with the golden mean has been dealt with in detail, we will consider only those cases where m and n in (8) are not both equal to unity. In our calculations, we define $x_l \equiv \frac{1}{2}\mathrm{Tr}\, \boldsymbol{M}_l$.

We now give some details for the recursion relations among the traces of the transfer matrices corresponding to several lattices which are generalisations of the Fibonacci lattice [20-22].

2.1. The silver mean

For this case, we set $m = 1$ and $n = 2$ in the recursion relation (8) and the ratio of successive Fibonacci numbers has the $\lim_{l\to\infty} F_{l+1}/F_l = 1 + 2^{1/2} \equiv \sigma_s$, the *silver mean.* We have

$$\boldsymbol{M}_{l+1} + \boldsymbol{M}_{l-1} = \boldsymbol{M}_{l-1}\boldsymbol{M}_l(\boldsymbol{M}_l + \boldsymbol{M}_l^{-1}). \tag{9}$$

Taking the trace of (9), we obtain

$$x_{l+1} = 4x_l t_{l+1} - x_{l-1} \tag{10a}$$

where $t_l \equiv \mathrm{Tr}(\boldsymbol{M}_{l-2}\boldsymbol{M}_{l-1})/4$. That is, the recursion relation in (10a) *cannot* be expressed in terms of x_l only. A recursion relation for t_l has been derived and the result is

$$t_{l+1} = x_{l-1}x_l - t_l. \tag{10b}$$

Equations (10) jointly define the dynamical map in three dimensions for the Fibonacci series with the silver mean. The initial conditions are $x_1 = \frac{1}{2}\mathrm{Tr}\, \boldsymbol{M}_A$, $x_2 = \frac{1}{2}\mathrm{Tr}(\boldsymbol{M}_A\boldsymbol{M}_B)$ and $t_3 = x_1(x_2 - \frac{1}{2}) - (V_A - V_B)/4$. Defining a three-dimensional vector by $\boldsymbol{r}_l = (x_l, y_l, z_l) = (x_l, x_{l+1}, t_{l+2})$, (10) can be written as a non-linear dynamical map

$$\boldsymbol{r}_{l+1} = F_s(\boldsymbol{r}_l) = [y_l, 4y_l z_l - x_l, y_l(4y_l z_l - x_l) - z_l]. \tag{11}$$

The invariant for the dynamical map in (10) can be derived in a rather straightforward way. Equation (10a) yields

$$x_{l+1}(x_{l+1}-4x_lt_{l+1}) = x_{l-1}(x_{l-1}-4x_lt_{l+1}) \tag{12}$$

where the factors in brackets on the left- and right-hand sides of (12) are simply $-x_{l-1}$ and $-x_{l+1}$, respectively. Adding x_l^2 to both sides of (12), and substituting for x_lx_{l+1} and $x_{l-1}x_l$ from (10b), we obtain after a little algebra the invariant for F_s in (11):

$$I_s = x_l^2+y_l^2+4z_l^2-4x_ly_lz_l-1. \tag{13}$$

Thus the orbits of (11) are confined on the same two-dimensional manifold as the dynamical system for the Fibonacci sequence with the golden mean. This manifold has a central part which is topologically similar to the surface of a sphere with four arms coming out of the sphere and moving out to infinity. In fact, from our initial conditions, we obtain $I_s=(V_A-V_B)^2/4$. Clearly, with $a\equiv(I_s+1)^{1/2}$, we have

$$A_s(0, 0, a/2)\rightarrow B_s(0, 0, -a/2)\rightarrow A_s.$$

That is, A_s and B_s are fixed points of F_s^2. We also have a four-cycle orbit:

$$C_s(0, a, 0)\rightarrow D_s(a, 0, 0)\rightarrow E_s(0, -a, 0)\rightarrow H_s(-a, 0, 0)\rightarrow C_s.$$

When $I_s=0$, the four arms just touch the central part and we can set $x_l=\cos\theta_l$ where θ_l is real and satisfies

$$\theta_{l+1}=2\theta_l+\theta_{l-1}. \tag{14}$$

Linearisation of F_s^2 and F_s^4 about their fixed points yields the Jacobian matrix of the mapping [26]. The eigenvalues and eigenvectors of the family of fixed points determine the stability and motion near the fixed points. The eigenvalues for the fixed points of period two are

$$\lambda=1 \qquad \lambda_\pm=-2a^2-1\pm2a(1+a^2)^{1/2}.$$

The eigenvalues of the fixed points of period four are

$$\lambda=1 \qquad \lambda_\pm=1-16a^2+32a^4\pm4a(4a^2-1)(4a^2-2)^{1/2}.$$

We note that, like the map with the golden mean, each family of fixed points has an eigenvalue $\lambda=1$. Also for both Fibonacci sequences, the Jacobian matrix has determinant equal to unity at every point in the map, implying that these maps are volume-preserving at every point in the iteration. The dynamical map for the trace of the transfer matrix in (11) is shown in figure 1. There are three major bands, as is the case for the map with the golden mean. In figure 2, the magnitude of the wavefunction given by (3) is plotted as a function of the lattice site number with the two kinds of hopping matrix elements chosen to satisfy $t_B/t_A=2.0$ and the energy $E=0$. The lattice corresponds to the Fibonacci sequence with the silver mean. The wavefunction is neither localised nor extended, like the Fibonacci lattice with the golden mean.

2.2. *The bronze mean*

When $m=1$ and $n=3$, the ratio of successive Fibonacci numbers F_{l+1}/F_l approaches the *bronze mean* $\sigma_\beta\equiv(3+13^{1/2})/2$. We obtain the dynamical map for this case by writing the recursion relation as

$$\boldsymbol{M}_{l+1}+(\boldsymbol{M}_{l-1}\boldsymbol{M}_l^{-1}+\boldsymbol{M}_{l-2}) = \boldsymbol{M}_{l-1}\boldsymbol{M}_l(\boldsymbol{M}_l^2+\boldsymbol{M}_l^{-2})+\boldsymbol{M}_{l-2}. \tag{15}$$

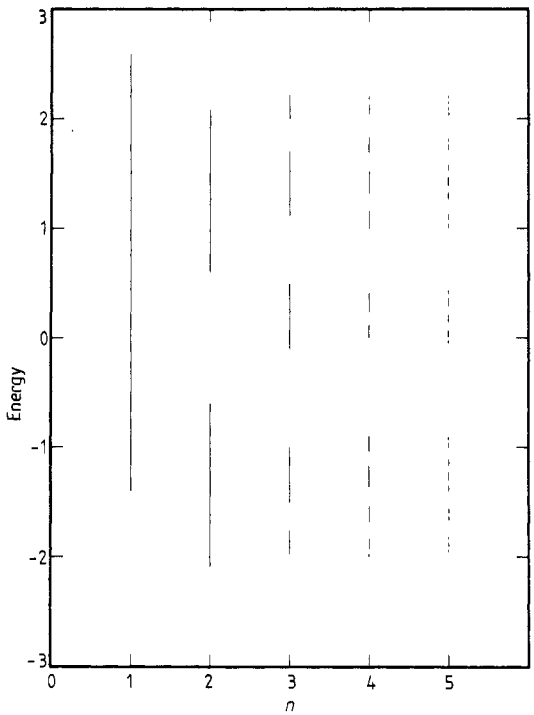

Figure 1. Band structure of (4) when $V_A = 0.6 = -V_B$ and the two values of the potential are arranged in the Fibonacci sequence with the silver mean.

Taking the trace of this equation we obtain after a little algebra

$$x_{l+1} + 2x_{l-1}g_l = (4x_l^2 - 2)g_{l+1} + x_{l-2} \tag{16}$$

where $g_l \equiv \frac{1}{2}\,\mathrm{Tr}(\boldsymbol{M}_{l-2}\boldsymbol{M}_{l-1})$. Equation (15) is consistent with

$$x_{l+1} = (4x_l^2 - 1)g_{l+1} - 2x_{l-1}x_l \tag{17a}$$

$$g_{l+1} = 2x_{l-1}(x_l - g_l) + x_{l-2} \tag{17b}$$

where x_1 and x_2 have the same values as for the Fibonacci series with the silver mean and $g_3 = 2x_1x_2 - x_1 + (V_B - V_A)/2$. By defining a three-dimensional vector $\boldsymbol{r}_l = (x_l, x_{l-1}, g_{l+1})$, (17) are alternatively expressed as $\boldsymbol{r}_{l+1} = F_\beta(\boldsymbol{r}_l)$ where F_β is a non-linear dynamical map given explicitly by

$$x_{l+1} = (4x_l^2 - 1)z_l - 2x_l y_l \qquad y_{l+1} = x_l \qquad z_{l+1} = 4x_l[(2x_l^2 - 1)z_l - x_l y_l] + y_l. \tag{18}$$

There is a conserved quantity associated with the mapping in (18). This quantity is given by the same form as the invariant for the silver mean except that $z_l \to z_l/2$. Thus we have verified that the recursion relation in (8) has the same invariant for $m = 1$ and $n = 1$, 2 and 3. The map F_β has a six-cycle orbit given by

$$A_\beta(0,0,b) \to B_\beta(-b,0,0) \to C_\beta(0,-b,0) \to D_\beta(0,0,-b) \to E_\beta(b,0,0) \to F_\beta(0,b,0) \to A_\beta$$

where $b = (I+1)^{1/2}$ and $I \equiv (V_A - V_B)^2/4$ is the constant of motion. It is easy to verify that F_β also has a two-cycle orbit given by

$$A_1(\tfrac{1}{2}, 0, \tfrac{1}{2}) \to A_2(0, \tfrac{1}{2}, -\tfrac{1}{2}) \to A_1.$$

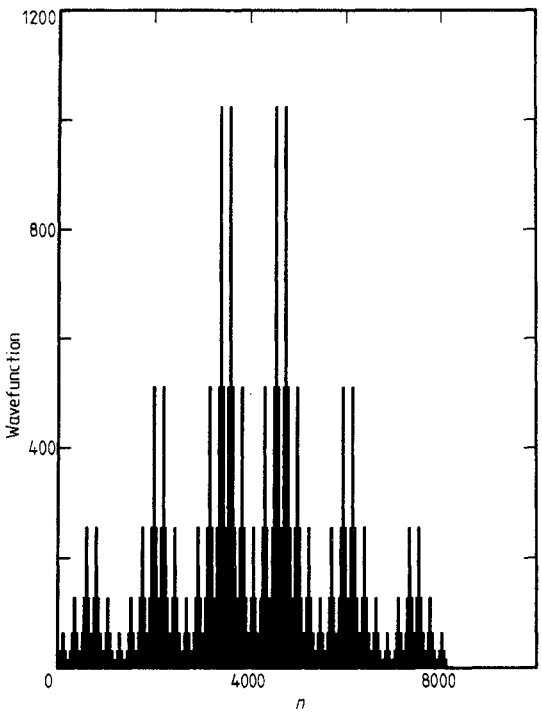

Figure 2. The magnitude of the electronic wavefunction $|\psi_n|$ at the centre of the band ($E=0$) for $t_B/t_A=2.0$. $|\psi_n|$ is plotted against site number n for the lattice with the silver mean. We choose $\psi_0=0$ and $\psi_1=1$ in the non-diagonal model in (3).

This calculation shows that the Jacobian matrix for the map in (18) has determinant equal to unity at every point in the iteration, like the maps corresponding to the Fibonacci sequences with the golden and silver mean. The magnitude of the wavefunction for the lattice with the bronze mean is plotted in figure 3 as a function of the lattice site number along the quasiperiodic direction for $E=0$ and t_B/t_A set equal to 2 in (3).

2.3. *The copper mean*

We now turn to the class of second-order Fibonacci lattices for which the invariant is not the same as it is for the two cases discussed above. This set is generated by setting $n=1$ in (8) and taking $m=2,3,\ldots$. When $m=2$ and $n=1$, F_{l+1}/F_l approaches the *copper* mean value $\sigma_c\equiv 2$. The trace map is obtained by taking the trace of

$$\boldsymbol{M}_{l+1}=(\boldsymbol{M}_{l-1}^2+\boldsymbol{M}_{l-1}^{-2})\boldsymbol{M}_l-\boldsymbol{M}_{l-1}^{-2}\boldsymbol{M}_l. \tag{19}$$

Equation (19) yields

$$x_{l+1}=(4x_{l-1}^2-2)x_l+\gamma \tag{20}$$

where $\gamma=-\frac{1}{2}\,\mathrm{Tr}(\boldsymbol{M}_{l-1}^{-2}\boldsymbol{M}_l)$. When l is replaced by $l+1$ in γ and the recursion relation for the matrices is used, a short calculation shows that γ is independent of l. Defining a two-dimensional vector by $\boldsymbol{r}=(x_l,y_l)\equiv(x_l,x_{l-1})$, (20) defines a mapping on the two-dimensional plane where γ remains unchanged for any orbit. The sequence with

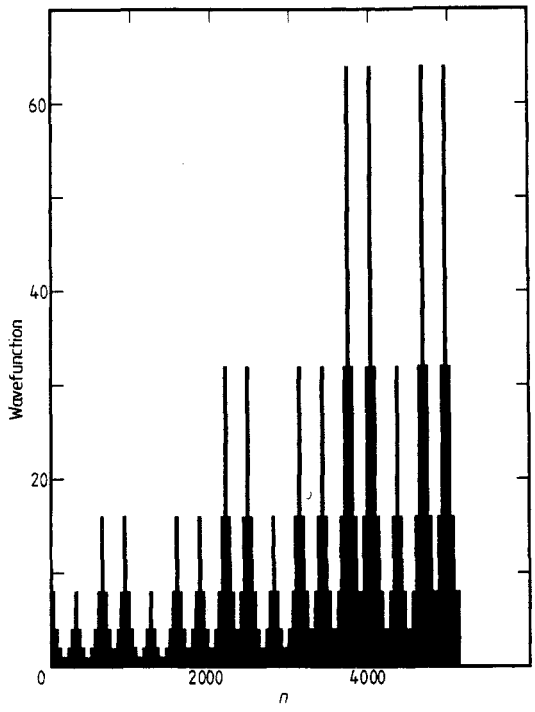

Figure 3. Same as figure 2 for the wavefunction at the centre of the band ($E = 0$) for the lattice with the bronze mean.

$S_1 = \{B\}$, $S_2 = \{A\}$, $S_3 = \{BBA\}$, and so on, has $\gamma = x_2 - 2x_1$. The map in (20) has a two-cycle orbit given by $(\frac{1}{4}, -1) \to (-1, \frac{1}{4})$. Setting $E = 0$, we find that the matrices are 4-cycle and are given by

$$\begin{aligned} \boldsymbol{M}_1 &= \begin{pmatrix} \frac{1}{2} & -1 \\ 1 & 0 \end{pmatrix} & \boldsymbol{M}_2 &= \begin{pmatrix} -2 & -1 \\ 1 & 0 \end{pmatrix} \\ \boldsymbol{M}_3 &= \begin{pmatrix} 1 & \frac{3}{4} \\ -1 & -\frac{1}{2} \end{pmatrix} & \boldsymbol{M}_4 &= \begin{pmatrix} -1 & \frac{5}{4} \\ 0 & -1 \end{pmatrix} \end{aligned} \tag{21}$$

with $\boldsymbol{M}_l = \boldsymbol{M}_{l+4}$. The 3-cycle of the trace given by $(\frac{1}{2}, -\frac{1}{4}) \to (-\frac{1}{4}, -1) \to (-1, \frac{1}{2})$ has a matrix 6-cycle which is

$$\begin{aligned} \boldsymbol{M}_1 &= \begin{pmatrix} 1 & -1 \\ 1 & 0 \end{pmatrix} & \boldsymbol{M}_2 &= \begin{pmatrix} -\frac{1}{2} & -1 \\ 1 & 0 \end{pmatrix} \\ \boldsymbol{M}_3 &= \begin{pmatrix} -1 & 0 \\ -\frac{3}{2} & -1 \end{pmatrix} & \boldsymbol{M}_4 &= \begin{pmatrix} 0 & -\frac{1}{2} \\ 2 & 1 \end{pmatrix} \\ \boldsymbol{M}_5 &= \begin{pmatrix} 0 & -\frac{1}{2} \\ 2 & -\frac{1}{2} \end{pmatrix} & \boldsymbol{M}_6 &= \begin{pmatrix} -1 & \frac{3}{4} \\ 0 & -1 \end{pmatrix} \end{aligned} \tag{22}$$

with $\boldsymbol{M}_l = \boldsymbol{M}_{l+6}$. We have verified that (20) has a four-cycle trace map with four-cycle matrix as well as a four-cycle trace map with an eight-cycle matrix. This abundance of cyclic orbits led us to investigate the values of x_1 and x_2 for which the orbits are

aperiodic or cyclic, i.e. bounded. Figure 4 shows the points which initiate bounded orbits and figure 5 shows a typical closed orbit. The Jacobian matrix for the fixed points of period two has eigenvalues

$$\lambda_{\pm} = \tfrac{1}{4}(-15 \pm 161^{1/2}).$$

The eigenvalues of the fixed points of period three, quoted above, are

$$\lambda_{\pm} = \tfrac{1}{8}[53 \pm 9(41)^{1/2}].$$

Both families of fixed points are saddle points and the value of the determinant of the Jacobian matrix depends on the point in the map where it is evaluated. That is, this map does not perserve the volume element locally and might be the reason why we have not been able to obtain a constant of motion. Figure 6 shows a plot of the band structure corresponding to the Fibonacci sequence with the copper mean. Unlike the band structure shown in figure 1, there are only *two* major sub-bands for this case. The magnitude of the wavefunction for this lattice is plotted in figure 7. It is clear that this wavefunction is localised, quite unlike the preceding cases corresponding to a binary string. However, the localisation in this model is not as strong as the (Anderson) localisation in the one-dimensional disordered system discussed by Mott and Twose [27]. For this kind of Anderson localisation, the envelope of the wavefunction decays exponentially from some point in space. Tong [28] has presented an example for the localisation of electronic states in a one-dimensional disordered system.

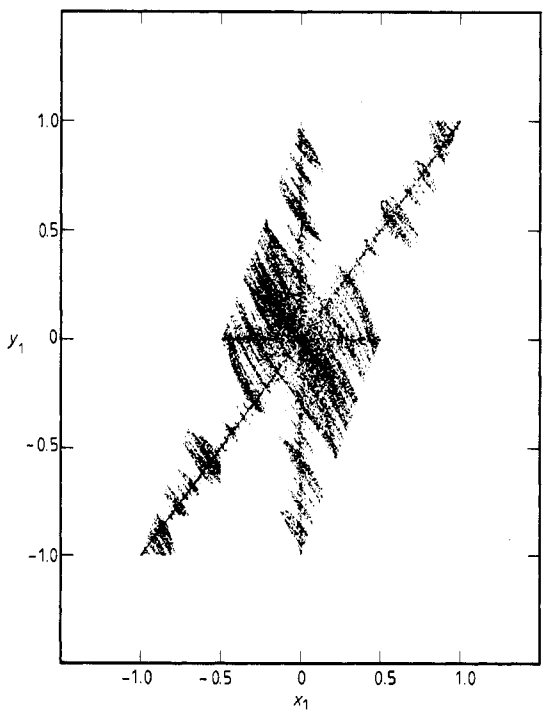

Figure 4. The set of initial points with coordinates (x_1, y_1) which yield bounded, i.e. cyclic or aperiodic, orbits for the map in (20).

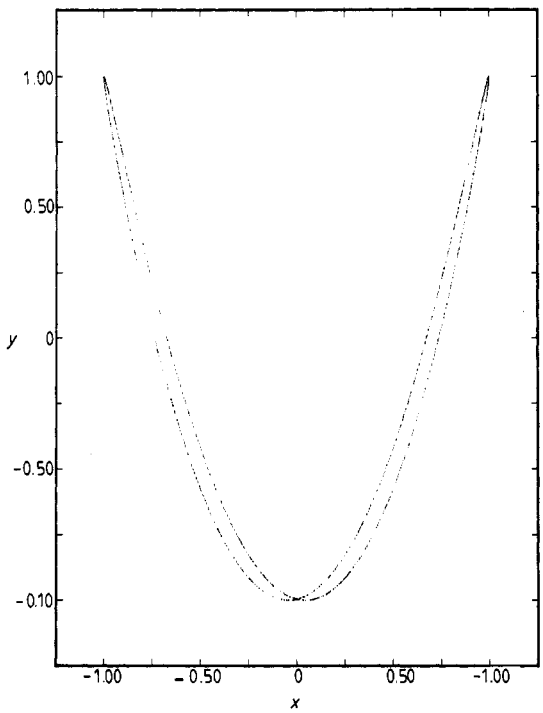

Figure 5. An aperiodic orbit for the copper mean map in (20) with $x_0 = 0$, $y_1 = -\frac{249}{250}$.

2.4. The nickel mean

When the Fibonacci numbers are given by $F_{l+1} = 3F_{l-1} + F_l$, the recursion relation for the transfer matrices is obtained by setting $m = 3$ and $n = 1$ in (8). In the limit $l \to \infty$, F_{l+1}/F_l tends to the nickel mean of $\sigma_n \equiv (1 + 13^{1/2})/2$. In this case we choose to take the trace of

$$\boldsymbol{M}_{l+1} + \boldsymbol{M}_{l-1}^{-3}\boldsymbol{M}_l = (\boldsymbol{M}_{l-1}^{3} + \boldsymbol{M}_{l-1}^{-3})\boldsymbol{M}_l \tag{23}$$

which gives

$$x_{l+1} = 2(4x_{l-1}^2 - 3)x_{l-1}x_l + \mu_l \tag{24}$$

where $\mu_l = -\frac{1}{2}\,\mathrm{Tr}(\boldsymbol{M}_{l-1}^{-3}\boldsymbol{M}_l)$. To obtain the recursion relation for μ_l we take the trace of

$$\boldsymbol{M}_{l-1}^{-3}\boldsymbol{M}_l = (\boldsymbol{M}_{l-1}^{-1} + \boldsymbol{M}_{l-1})\boldsymbol{M}_{l-1}^{-2}\boldsymbol{M}_l - \boldsymbol{M}_l^{-1}\boldsymbol{M}_{l-2}^{3}\boldsymbol{M}_l \tag{25}$$

where (25) follows directly from the recursion relation for the transfer matrices. After a little algebra, we obtain from (25)

$$\mu_l = 2x_{l-1}\mu_{l-1} + x_{l-2}(4x_{l-2}^2 - 3). \tag{26}$$

Equations (24) and (26) can be written compactly as

$$x_{l+1} = 2x_lT_l + G_l \tag{27a}$$

$$G_{l+1} = 2x_lG_l + T_l \tag{27b}$$

$$T_{l+1} = (4x_l^2 - 3)x_l. \tag{27c}$$

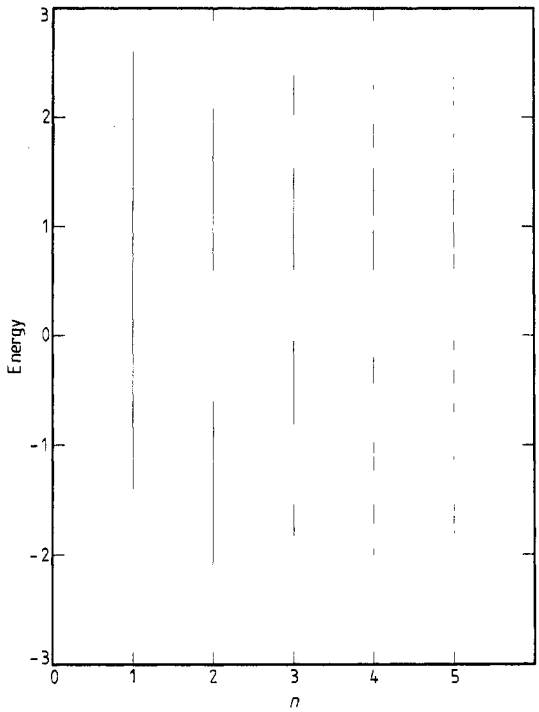

Figure 6. Band structure of the discrete Schrödinger equation when $V_A = 0.6 = -V_B$. The sequence of potentials is arranged according to the Fibonacci sequence with the copper mean.

By defining a three-dimensional vector $\boldsymbol{r}_l = (x_l, T_l, G_l)$, (27) define a three-dimensional map $\boldsymbol{r}_{l+1} = \boldsymbol{F}_n(\boldsymbol{r}_l)$ which is given explicitly by

$$x_{l+1} = 2x_l y_l + z_l \qquad y_{l+1} = (4x_l^2 - 3)x_l \qquad z_{l+1} = 2x_l z_l + y_l. \tag{28}$$

The map in (28) has fixed points of period three given by

$$A_n(\tfrac{1}{2}, 1, -\tfrac{1}{2}) \to B_n(\tfrac{1}{2}, -1, \tfrac{1}{2}) \to C_n(-\tfrac{1}{2}, -1, -\tfrac{1}{2}).$$

The eigenvalues of this family of fixed points are

$$\lambda = 0 \qquad \lambda_\pm = 5 \pm 2(13)^{1/2}. \tag{29}$$

The map also has a fixed point of period one with coordinates $(-\frac{1}{2}, 1, \frac{1}{2})$. The eigenvalues of the Jacobian matrix for this point are

$$\lambda = 0 \qquad \lambda_\pm = \tfrac{1}{2}(1 \pm 13^{1/2}). \tag{30}$$

All these fixed points are saddle points and the determinant of the Jacobian at these fixed points is zero. That is, this map is non-invertible at the fixed points. In figure 8, we plot the initial points which give rise to bounded orbits for the *nickel* map and has some similarities with the plot in figure 7.

2.5. A mixed case

In view of the numerical results given above for the Fibonacci lattices with the silver and copper means, we now turn to the *mixed* case for which the recursion relation is

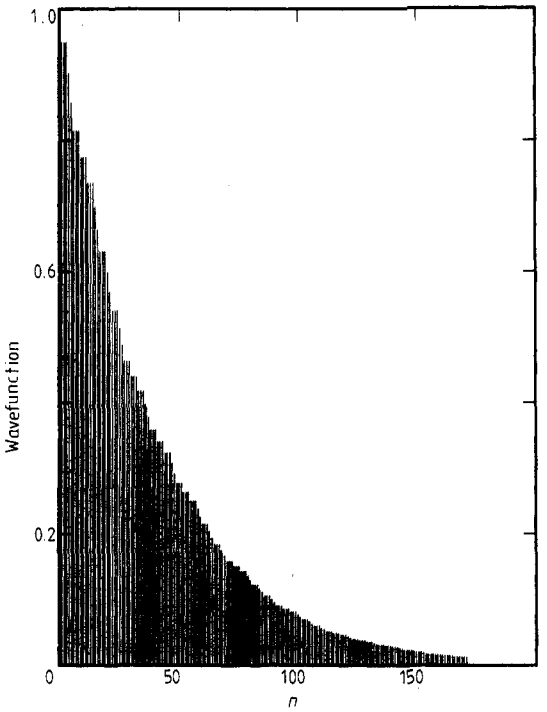

Figure 7. Same as figure 2 except that the lattice is arranged according to the Fibonacci sequence with the copper mean and $t_B/t_A = 0.95$.

given by

$$\boldsymbol{M}_{l+1} = \boldsymbol{M}_{l-1}^2 \boldsymbol{M}_l^2. \tag{31}$$

This, in some sense, corresponds to a combination of two types of Fibonacci series. Our main interest is to see whether the orbits are more like those for the copper mean or silver mean. Rewriting (31) as

$$\boldsymbol{M}_{l+1} + \boldsymbol{M}_{l-1}^2 = \boldsymbol{M}_{l-1}^2 \boldsymbol{M}_l (\boldsymbol{M}_l + \boldsymbol{M}_l^{-1}) \tag{32}$$

and taking the trace of (32), we obtain

$$x_{l+1} = (4x_{l-1}^2 - 1)(2x_{l-1}^2 - 1) - 2x_l(2x_{l-2}^2 - 1). \tag{33}$$

A collection of the initial points for which the orbits are bounded is shown in figure 9. Thus the map defined in (29) has a behaviour similar to that of the map with the copper mean. It is not clear that this should be so but we have managed to identify the nature of the map through numerical calculations. Also, the determinant for the Jacobian matrix corresponding to the map in (33) depends on the coordinates of the point in the iteration. Figure 8 shows a plot of the points which initiate bounded orbits.

3. Quasiperiodic dynamics of a third-order Fibonacci lattice

We now carry out calculations to obtain the recursion relations among the traces of transfer matrices corresponding to a third-order Fibonacci lattice.

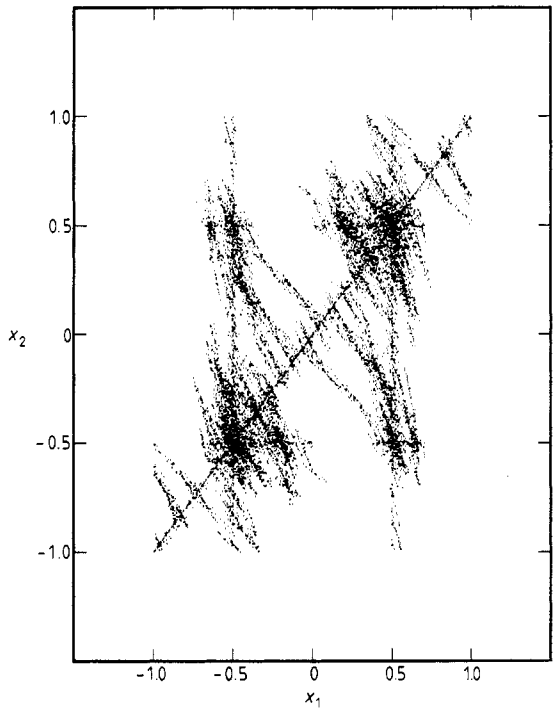

Figure 8. Same as figure 4, except that the dynamical map is given by (27) corresponding to the Fibonacci sequence with the nickel mean.

The third-order Fibonacci numbers are generated by adding the three preceding numbers. They are given by $F_{l+1}=F_{l-2}+F_{l-1}+F_l$ for $l\geqslant 2$ with $F_0=F_1=F_2=1$. Closed-form analytic results for F_l can be obtained and calculation shows that, in the limit as $l\to\infty$, F_{l+1}/F_l tends to the mean value $\sigma_t=\frac{1}{3}(1+\gamma_+^{1/3}+\gamma_-^{1/3})$, where $\gamma_\pm=19\pm 297^{1/2}$. For the three building blocks A, B and C the sequence is constructed by $S_{l+1}=\{S_{l-2}S_{l-1}S_l\}$ for $l\geqslant 3$ with $S_1=\{C\}$, $S_2=\{ABC\}$ and $S_3=\{BCABC\}$. The inflation transformation for this sequence is therefore $C\to ABC$, $B\to C$ and $A\to B$. $\boldsymbol{M}_l$ satisfies the recursion formula

$$\boldsymbol{M}_{l+1}=\boldsymbol{M}_{l-2}\boldsymbol{M}_{l-1}\boldsymbol{M}_l. \tag{34}$$

The energy excitation spectrum is calculated by determining those energies for which the corresponding wavefunctions ψ_l do not increase as l increases. Since the matrices $\boldsymbol{M}_l$ are unimodular, the condition that the energy is allowed could be transferred to the trace of the transfer matrix which must satisfy the relation $\mathrm{Tr}\,\boldsymbol{M}_l<2$. We now convert (34) into a very simple recursion relation for $x_l=\frac{1}{2}\,\mathrm{Tr}\,\boldsymbol{M}_l$ by taking the trace of the equation

$$\boldsymbol{M}_{l+1}+\boldsymbol{M}_{l-3}^{-1}=\boldsymbol{M}_{l-2}\boldsymbol{M}_{l-1}(\boldsymbol{M}_l+\boldsymbol{M}_l^{-1}). \tag{35}$$

Since $\boldsymbol{M}_l$ is a 2×2 matrix with determinant equal to unity, (35) yields for $l\geqslant 2$

$$x_{l+1}=4x_lG_l-x_{l-3} \tag{36}$$

where $G_l=\frac{1}{4}\mathrm{Tr}(\boldsymbol{M}_{l-2}\boldsymbol{M}_{l-1})$. The recursion relation for G_l is obtained by taking the trace of the equation

$$\boldsymbol{M}_{l-2}\boldsymbol{M}_{l-1}+\boldsymbol{M}_{l-4}\boldsymbol{M}_{l-3}=\boldsymbol{M}_{l-1}(\boldsymbol{M}_{l-1}^{-1}\boldsymbol{M}_{l-2}\boldsymbol{M}_{l-1}+\boldsymbol{M}_{l-2}^{-1}) \tag{37}$$

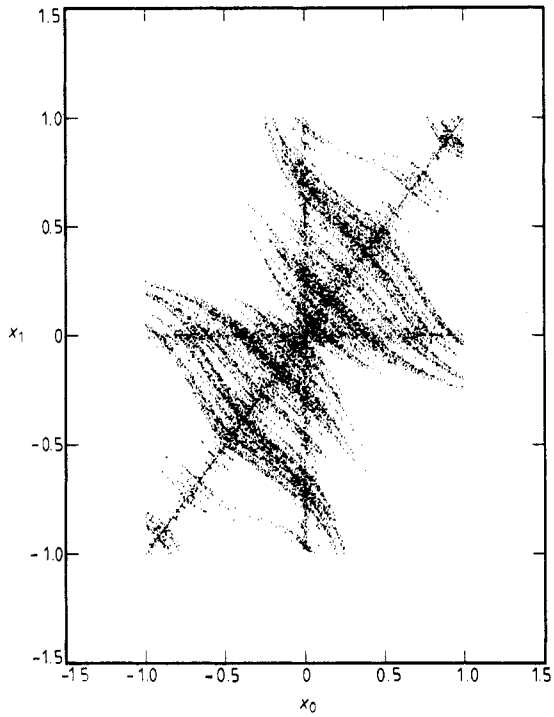

Figure 9. Same as figure 4, except that the dynamical map is given by (33).

which follows directly from (34). After a little algebra, (37) gives

$$G_l = x_{l-1}x_{l-2} - G_{l-2}. \tag{38}$$

Equations (36) and (38) jointly give the dynamical map in six-dimensional space for the third-order Fibonacci series defined in (34). This map is given in terms of the six-dimensional vector $\boldsymbol{r}_l \equiv (w_l, y_l, g_l, X_l, z_l, v_l)$ where, for convenience, we define $X_l = 2x_l$ and $g_l = 4G_l$. It is a simple matter to show that the dynamical map defined by (36) and (38) are consistent with the transformation

$$w_{l+1} = g_l \qquad y_{l+1} = X_l \qquad g_{l+1} = X_l y_l - w_l$$
$$X_{l+1} = X_l g_l - v_l \qquad z_{l+1} = y_l \qquad v_{l+1} = z_l.$$

The Jacobian matrix for this mapping has a determinant equal to unity and so it too is volume-preserving like the class of Fibonacci sequences which the map with the golden mean belongs to. In figure 10, we plot the wavefunction at the centre of the band of the non-diagonal model in (3) with $t_A = 2$, $t_B = 1$ and $t_C = 0.5$. The initial conditions for the ternary map (diagonal model) are

$$x_{-1} = \tfrac{1}{2}\,\mathrm{Tr}\,(\boldsymbol{M}_A) \qquad x_0 = \tfrac{1}{2}\,\mathrm{Tr}(\boldsymbol{M}_B) \qquad x_1 = \tfrac{1}{2}\,\mathrm{Tr}(\boldsymbol{M}_C)$$
$$x_2 = 4x_{-1}x_0x_1 - x_{-1} - x_0 - x_1 \tag{39}$$
$$G_0 = \tfrac{1}{2} \qquad G_1 = x_{-1}x_0 - \tfrac{1}{2}$$

It is a simple matter to show that $x_l = 0, \pm 1$ are (trivial) fixed points with unit cycle for (36) and (38). Setting $x_{-1} = x_0 = x_1 = x$ where $|x| < 1$, numerical calculations show that the resulting values of x_l satisfy $|x_l| < 1$ for all l. For example, when the initial

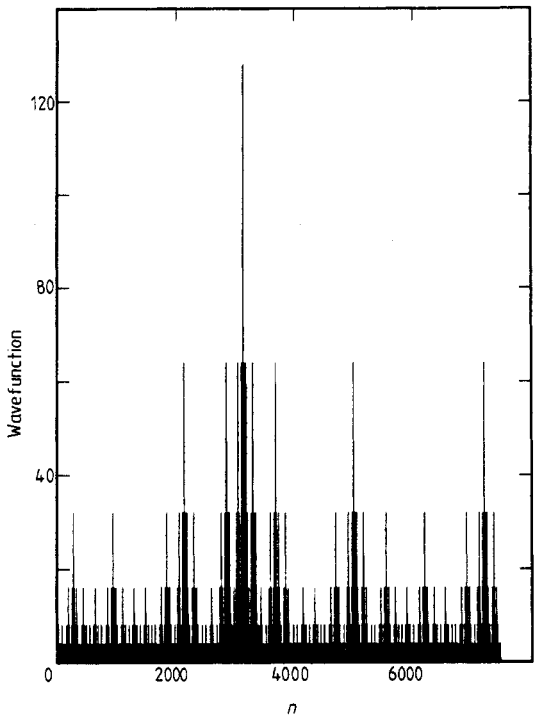

Figure 10. The magnitude of the wavefunction ($|\psi_n|$) at the centre of the band of the non-diagonal model of the Schrödinger equation. The hopping matrix elements are chosen as $t_A = 2$, $t_B = 1$ and $t_C = 0.5$ in the third-order Fibonacci sequence.

points are chosen as $\pm 2^{1/2}$, the cycle is $x_l = x_{l+8}$ and $\boldsymbol{M}_l = \boldsymbol{M}_{l+8}$. We have carried out an extensive search for the initial points x_{-1}, x_0 and x_1 which give rise to bounded orbits. We have not been able to find any more points besides the ones along the diagonal (1, 1, 1) of the cube and the trivial fixed points.

4. Transmission of light through quasiperiodic media

In a recent paper, Kohmoto *et al* [29] proposed an experiment for light transmission through a multilayer medium arranged according to the Fibonacci sequence. The medium is assumed to be translationally invariant in the plane perpendicular to the superlattice direction of growth and is bounded on either side by a homogeneous semi-infinite medium. In this section, we obtain the transmission coefficient of a transverse electric wave which is incident on a medium constructed according to a *generalised* Fibonacci sequence with vacuum on one side and a dielectric on the other simulating the effect of a substrate.

We take the thickness of the lth layer as d_l and its refractive index as n_l. Let θ_l be the angle which light makes with the normal to the interface when travelling within the lth layer. The transfer matrix relating the amplitudes of the electric vectors on opposite sides of this dielectric slab is [30]

$$\boldsymbol{M}(n_l) = \begin{pmatrix} \cos\beta_l & -\mathrm{i}p_l^{-1}\sin\beta_l \\ -\mathrm{i}p_l\sin\beta_l & \cos\beta_l \end{pmatrix} \tag{40}$$

where the optical phase length $\beta_l = kn_l d_l \cos\theta_l$, $p_l = n_l \cos\theta_l$ and k is the wavenumber of the incident beam of light in vacuum. Clearly, $\boldsymbol{M}(n_l)$ is unimodular. The transfer matrix through N layers is also unimodular and given by

$$\boldsymbol{M}_N = \prod_{i=1}^{N} \boldsymbol{M}(n_l) = \begin{pmatrix} M_{11} & M_{12} \\ M_{21} & M_{22} \end{pmatrix}. \tag{41}$$

Assuming that p_0 is the value of p_l in vacuum and p_S is the value in the other medium adjacent to the superlattice, calculation shows that the transmission coefficient is given by

$$T = 4p_0^2[\, p_0^2 M_{11}^2 + p_S^2 M_{22}^2 + (p_0 p_S)^2 |M_{12}|^2 + |M_{21}|^2 + 2p_0 p_S]^{-1} \tag{42}$$

For light propagation through a multilayer medium arranged according to a third-order Fibonacci sequence of $N = F_j$ layers, the matrix in (41) is calculated according to (34), with the initial values

$$\begin{aligned} \boldsymbol{M}_1 &= \boldsymbol{M}_C \\ \boldsymbol{M}_2 &= \boldsymbol{M}_{CA}\boldsymbol{M}_{AB}\boldsymbol{M}_C \\ \boldsymbol{M}_3 &= \boldsymbol{M}_{CB}\boldsymbol{M}_C\boldsymbol{M}_2. \end{aligned} \tag{43}$$

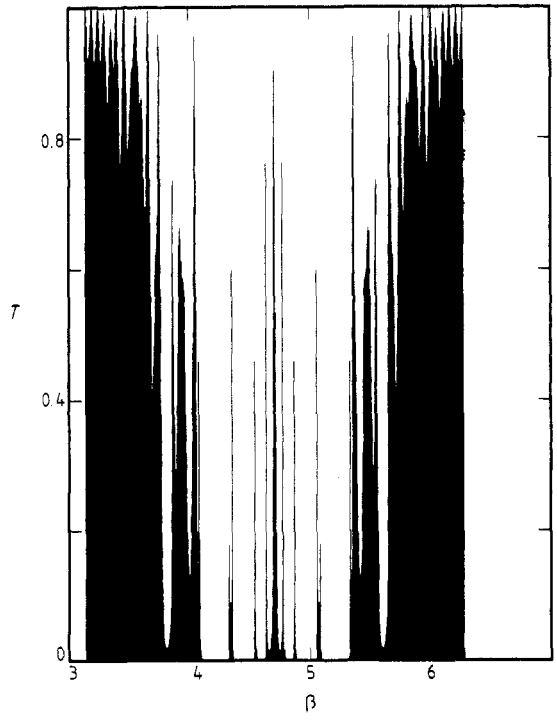

Figure 11. Plot of the transmission coefficient T as a function of the optical phase length β for normal incidence. The layered medium has F_7(= 57 layers) and is arranged according to the third-order Fibonacci sequence defined in (34). The indices of refraction are chosen as $n_A = 2$, $n_B = 3$ and $n_C = 1.5$.

Here, $\boldsymbol{M}_C$ is the matrix in (40) for propagation through a medium of type C, whereas $\boldsymbol{M}_{CA}$ stands for the matrix where light is passing through a type-A material after emerging from a material of type C. Similar definitions for $\boldsymbol{M}_{AB}$ and $\boldsymbol{M}_{CB}$ apply. The Fibonacci multilayer is sandwiched by two media made from type-C material.

The results in (40)-(43) apply for an arbitrary angle of incidence, wavenumber k and thickness of the layers. In order to simplify the book-keeping involved in numerical calculations, we have taken the incident light to be normal and the thickness of the layers to be such that $kn_Ad_A = kn_Bd_B = kn_Cd_C = \beta$. A plot of T against β when $p_0 = p_S = 1.5$ in (42) and $n_A = 2$, $n_B = 3$ and $n_C = 1.5$ is presented in figure 11, for a chain with $F_7 = 57$ sites. In order to better understand the effect of quasiperiodicity on the transmissivity of the medium, we have plotted T in figure 12 as a function of β for a periodic superlattice consisting of thirty AB blocks, i.e. sixty layers. The multilayer is sandwiched by two media of material of type C. The indices of refraction for the various types of material are the same as those chosen in figure 11. It is clear from figure 12 that there is only one range of values of the optical phase length β for which the transmission coefficient is negligible. There are, however, several ranges of film thickness which yield total reflection for the third-order Fibonacci lattice. The occurrence of total reflectivity of a multilayer system has been known for some time but the effect due to quasiperiodicity on the transmissivity is not fully understood. It is found that total reflectivity occurs around $\beta = (m+\frac{1}{2})\pi$ for the periodic multilayer. This feature appears to be independent of the values chosen for the refractive indices of the blocks or the thickness of the slab.

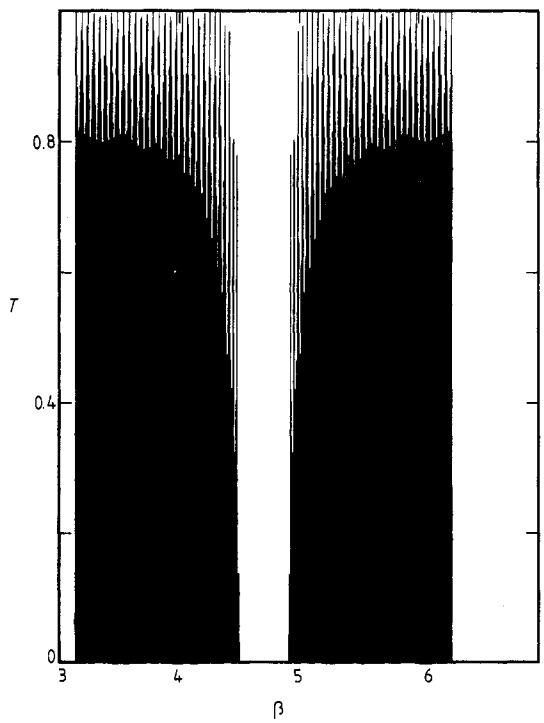

Figure 12. The transmission coefficient T plotted against the optical phase length β for normal incidence. There are 60 layers consisting of 30 AB blocks forming a periodic lattice. The indices of refraction are $n_A = 2$ and $n_B = 3$.

5. Resistance of a one-dimensional Fibonacci lattice

Several years ago, Anderson [31] pointed out that the electronic wavefunction in a macroscopic sample becomes localised if the randomness in the potential is sufficiently strong. Subsequently, the conceptual framework of a scaling description of the localisation problem was presented by Thouless and co-workers [33]. Assuming that the states near the Fermi level are localised and the occupied states of the spectrum form a dense set, the scaling theory states that the electrical resistance grows exponentially with sample size. Quasiperiodic systems, however, can have states which are either extended, localised or critical. Since the localisation length ξ is not well defined for critical states (in some sense, ξ is infinite), it is of interest to study the behaviour of the electrical resistance as a function of the length of the one-dimensional lattice. In this section, we calculate the electrical resistance of a one-dimensional quasicrystal with off-diagonal non-periodicity described by the tight-binding Hamiltonian in (3). The chain is assumed to have N lattice sites and the dimensionless resistance is defined by the Landauer [34] formula as the ratio of the reflection coefficient to the transmission coefficient. Recently, some questions have been raised by Sutherland and Kohmoto [35] concerning the suitability of the Landauer formula for a quasiperiodic system. These objections are justifiable since the energy spectrum is singularly continuous, i.e. the energy gaps are dense everywhere in the spectrum which means that linear response to an external electric field is not well defined. Therefore, treating the resistance as a means of characterising the electronic states, we use the Landauer formula and assume that only one scattering channel is available. Calculation shows that the Landauer resistance is given by [36, 37]

$$\rho = \frac{1}{4\sin^2 k}\left[\|\boldsymbol{M}_N\|^2 + 2(\cos k)(\boldsymbol{M}_N^{11} - \boldsymbol{M}_N^{22})(\boldsymbol{M}_N^{12} - \boldsymbol{M}_N^{21}) - 4(\cos^2 k)\boldsymbol{M}_N^{12}\boldsymbol{M}_N^{21} - 2\right]. \tag{44}$$

Here, $\|\boldsymbol{M}_N\|^2$ is the sum of the squares of the elements of the 2×2 matrix $\boldsymbol{M}_N = \boldsymbol{M}(N)$ defined by

$$\boldsymbol{M}(N) = \boldsymbol{M}(t_{N+1}, t_N)\boldsymbol{M}(t_N, t_{N-1}) \ldots \boldsymbol{M}(t_2, t_1) \tag{45}$$

where

$$\boldsymbol{M}(t_i, t_j) \equiv \begin{pmatrix} E/t_i & -t_j/t_i \\ 1 & 0 \end{pmatrix}. \tag{46}$$

In (44), the energy is defined in terms of the wavenumber k by $E = 2t_0 \cos k$ where the hopping matrix elements are equal to t_0 outside the disordered segment $1 \leqslant l \leqslant N$. Figure 13 shows a plot of the resistance ρ in (44) when the energy $E = 0$ and the hopping matrix elements take on values t_A and t_B arranged according to the Fibonacci sequence with the silver mean and $t_B/t_A = 2.0$. Clearly, the resistance ρ has a discrete structure and has a power law behaviour which is known for the Fibonacci lattice with the golden mean. These numerical results show that the features in the resistance obtained by Schneider *et al* [36] and Sutherland and Kohmoto [35] are not unique to

† For a review of the work carried out on the properties of disordered electronic systems, see [32].

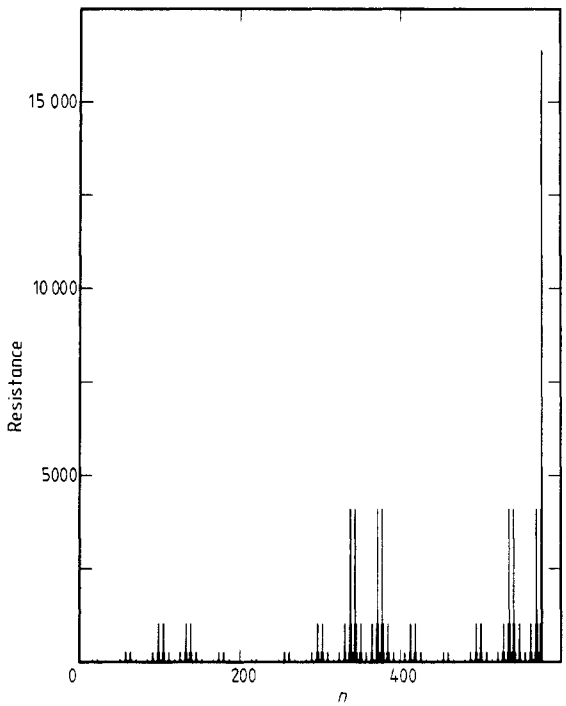

Figure 13. Plot of the resistance of a one-dimensional quasicrystal as a function of the number of sites in the chain. The energy is at the centre of the band and the Fibonacci sequence has the silver mean with $t_B/t_A = 2.0$.

the golden mean case but appears to be typical for the quaiperiodic arrays belonging to the family of Fibonacci sequences [38-41].

6. Summary

In this paper we have computed the recursion relations among the traces of transfer matrices corresponding to several lattices which are extensions of the Fibonacci case with the golden mean. There are some other papers dealing with extensions of quasicrystal models [38, 40-42]. In [42], Bombieri and Taylor have studied the conditions of quasiperiodicity in one-dimensional lattices.

The main points to focus on are as follows.

(i) The trace maps of the golden, silver and bronze mean lattices are volume-preserving while those of the copper and nickel mean lattices are volume-non-preserving. Unlike the volume-preserving class, the volume-non-preserving lattices are found to have a surprisingly large number of bounded orbits for the trace maps, implying the possible existence of attractors. These lattices also have localised states.

(ii) The third-order Fibonacci lattice discussed here has a map which is volume-preserving.

(iii) Light transmission through a multilayer medium arranged according to a generalisation of the Fibonacci sequence has been studied theoretically. We find several

ranges of film thickness for which there is total reflection for the third-order Fibonacci lattice.

(iv) The resistance of the third-order Fibonacci lattice has a similar power law behaviour as the Fibonacci lattice with the golden mean.

Recently, experiments have been carried out on Fibonacci superlattices. Merlin *et al* [43] analysed quasiperiodic GaAs-(AlGa)As by x-ray and Raman scattering experiments. Dharma-wardana *et al* [44] reported a study of Raman scattering from acoustic phonons in Si-Ge_xSi_{1-x} strained-layer Fibonacci superlattices. Also Karkut *et al* [45] reported on similar experiments for superconducting Mo-V superlattices. Behrooz *et al* [46] have measured the superconducting transition temperature as a function of magnetic field of thin (500 Å) Al wires arranged in quasicrystalline arrays. It remains to be seen whether lattices having volume-preserving and volume-non-preserving trace maps discussed in this paper would lead to any measurable quantities which have different characteristics from those arising from other types of quasiperiodic lattices.

Acknowledgments

This work was supported by grants from the Natural Sciences and Engineering Research Council of Canada and by the University of Lethbridge Research Fund.

References

[1] Kohmoto M, Kadanoff L P and Tang C 1983 *Phys. Rev. Lett.* **50** 1870
[2] Ostlund S, Pandit R, Rand D, Schellnhuber H J and Siggia E *Phys. Rev. Lett.* **50** 1873
[3] Ostlund S and Pandit R *Phys. Rev. B* **29** 1394
[4] Simon B 1987 *Adv. Appl. Math.* **3** 463
[5] Sokoloff J B 1985 *Phys. Rep.* **126** 189
[6] Kohmoto M *Phys. Rev. Lett.* **51** 1198
[7] Kohmoto M and Oono Y 1984 *Phys. Lett.* **102A** 145
[8] Luck M and Petritis D 1986 *J. Stat. Phys.* **42** 289
[9] Nori F and Rodriguez J P 1986 *Phys. Rev.* B **34** 2207
[10] Kohmoto M and Banavar J 1986 *Phys. Rev.* B **34** 563
[11] Lu J P Odagaki T and Birman J L 1986 *Phys. Rev.* B **33** 4809
[12] Kohmoto M, Sutherland B and Tang C 1987 *Phys. Rev.* B **35** 1020
[13] Sutherland B 1986 *Phys. Rev. Lett.* **57** 770
[14] Casdagli M 1986 *Commun. Math. Phys.* **107** 295
[15] Delyon F and Petritis D 1986 *Commun. Math. Phys.* **103** 441
[16] Sütö A 1986 *Commun. Math. Phys.* **103** 441
[17] Kohmoto M 1986 *Int. J. Mod. Phys.* B **1** 31
[18] Riklund R, Severin M and Liu Y 1987 *Int. J. Mod. Phys.* B **1** 121
[19] Verges J A, Brey L, Louis E and Tejedor C 1987 *Phys. Rev.* B **35** 5270
[20] Gumbs G and Ali M K 1988 *Phys. Rev. Lett.* **60** 1081
[21] Gumbs G and Ali M K 1988 *J. Phys. A Math. Gen* **21** L517
[22] Ali M K and Gumbs G 1988 *Phys. Rev.* B **38** 7091
[23] Hofstadter D R 1976 *Phys. Rev.* B **14** 2239
[24] Avron J and Simon B 1982 *Bull. Am. Math. Soc.* **6** 81
[25] Niu Q and Nori F 1986 *Phys. Rev. Lett.* **57** 2057
[26] Lichtenberg A J and Lieberman M A 1983 *Regular and Stochastic Motion* (Berlin Springer) p 183
[27] Mott N F and Twose W D 1961 *Adv. Phys.* **10** 107
[28] Tong B Y 1970 *Phys. Rev.* A **1** 52
[29] Kohmoto M, Sutherland B and Iguchi K 1987 *Phys. Rev. Lett.* **58** 2436
[30] Born M and Wolf E 1980 *Principles of Optics* (Oxford: Pergamon) § 1.6

[31] Anderson P W 1958 *Phys. Rev.* **109** 1492
[32] Lee P A and Ramakrishnan T V 1985 *Rev. Mod. Phys.* **57** 287
[33] Thouless D J 1974 *Phys. Rep.* **13** 93
[34] Landauer R 1970 *Phil. Mag.* **21** 863
[35] Sutherland B and Kohmoto M 1987 *Phys. Rev.* B **36** 5877
[36] Schneider T, Politi A and Würtz D 1987 *Z. Phys.* B **66** 469
[37] Stone A D, Joannopoulos J D and Chadi D J 1981 *Phys. Rev.* B **24** 5583
[38] Fujita M and Machida K 1987 *J. Phys. Soc. Japan* **56** 1470
[39] Schröeder M R 1984 *Number Theory in Science and Communication* (Berlin: Springer)
[40] Nori F, Niu Q, Fradkin E and Chang S J 1987 *Phys. Rev.* B **36** 8338
[41] Aubry S, Godreche C and Luck J M 1987 *Europhys. Lett.* **4** 639; 1985 *J. Stat. Phys.* submitted.
[42] Bombieri E and Taylor J E 1986 *J. Physique Colloq.* **47** C-3, 19
[43] Merlin R, Bajema K, Clarke R, Juang F Y and Bhattacharaya P K 1985 *Phys. Rev. Lett.* **55** 1768
[44] Dharma-wardana M W C, MacDonald A H, Lockwood D J, Baribeau J M and Houghton D C 1987 *Phys. Rev. Lett.* **58** 1761
[45] Karkut M G, Triscone J M, Ariosa D and Fisher Ø 1986 *Phys. Rev.* B **34** 4390
[46] Behrooz A, Burns M J, Deckman H, Levine D, Whitehead B and Chaikin P M 1980 *Phys. Rev. Lett.* **57** 368